

## Article

# Louvered Fin-and-Flat Tube Compact Heat Exchanger under Ultrasonic Excitation

Amin Amiri Delouei <sup>1,\*</sup>, Hasan Sajjadi <sup>1</sup>, Meysam Atashafrooz <sup>2</sup>, Mohammad Hesari <sup>1</sup>,  
Mohamed Bechir Ben Hamida <sup>3,4,5,\*</sup> and Ahmad Arabkoohsar <sup>6,7</sup>

<sup>1</sup> Mechanical Engineering Department, University of Bojnord, Bojnord 9453155111, Iran

<sup>2</sup> Mechanical Engineering Department, Sirjan University of Technology, Sirjan 7813733385, Iran

<sup>3</sup> College of Engineering, Department of Mechanical Engineering, Imam Mohammad Ibn Saud Islamic University (IMSIU), Riyadh 11432, Saudi Arabia

<sup>4</sup> Research Laboratory of Ionized Backgrounds and Reagents Studies (EMIR), Preparatory Institute for Engineering Studies of Monastir (IPEIM), University of Monastir, Monastir 5019, Tunisia

<sup>5</sup> Higher School of Sciences and Technology of Hammam Sousse (ESSTHS), Department of Physics, University of Sousse, Sousse 4011, Tunisia

<sup>6</sup> Department of Civil and Mechanical Engineering, Technical University of Denmark, 2800 Lyngby, Denmark

<sup>7</sup> Department of Energy, Aalborg University, 9220 Aalborg, Denmark

\* Correspondence: a.amiri@ub.ac.ir or a.a.delouei@gmail.com (A.A.D.); benhamida\_mbechir@yahoo.fr (M.B.B.H.)

**Abstract:** Utilizing ultrasonic excitation as an active method for studying the rate of heat transfer has gained considerable attention recently. The present study investigated the effects of ultrasonic excitation on the heat transfer rate in a fin-and-flat tube heat exchanger experimentally. The performance of the heat exchanger was investigated with and without the presence of ultrasonic excitation. A comprehensive parameter study was attempted, so several parameters, including ambient temperature, flow rate, air passing velocity, Reynolds number, and Nusselt number, were studied in a relatively wide range. An adequate uncertainty test, as well as a validation assessment, is provided to certify the credibility of the obtained results and the hired facility. The results revealed that reducing the flow rate, ambient temperature, and air passing velocity on the heat exchanger increased the ultrasonic excitation's effects. The highest heat transfer enhancement in the present experiment was 70.11%, measured at the lowest air passing velocity and ambient temperature with a Reynolds number 2166. The data presented in this paper will be useful for the optimal design of ultrasonic vibrating fin-and-tube heat exchangers.

**Keywords:** heat transfer; finned tube heat exchanger; ultrasonic excitation; active method; experimental study



**Citation:** Amiri Delouei, A.; Sajjadi, H.; Atashafrooz, M.; Hesari, M.; Ben Hamida, M.B.; Arabkoohsar, A. Louvered Fin-and-Flat Tube Compact Heat Exchanger under Ultrasonic Excitation. *Fire* **2023**, *6*, 13. <https://doi.org/10.3390/fire6010013>

Academic Editor: Ali Cemal Benim

Received: 15 December 2022

Revised: 19 December 2022

Accepted: 25 December 2022

Published: 31 December 2022



**Copyright:** © 2022 by the authors. Licensee MDPI, Basel, Switzerland. This article is an open access article distributed under the terms and conditions of the Creative Commons Attribution (CC BY) license (<https://creativecommons.org/licenses/by/4.0/>).

## 1. Introduction

The heat exchanger (HE) is one the foremost critical engineering tools and is used in both heating and cooling processes in several domestic, industrial, and commercial applications, including the wastewater treatment, HVAC, waste heat recovery units, and pharmaceutical industries [1]. HEs are used to fulfilling different tasks in the industry depending on the type of fluid, density, viscosity, and temperature. Waste of energy in practice is a common phenomenon that could be recovered by means of HEs and heat a different stream in the process [1]. This can be seen as a practical way to save money and avoid employing an external energy source, which is generally expensive and harmful to the environment.

The need for heat transfer is a thorny issue in HEs and can be investigated by looking into many factors, such as structure complexity, intermediate fluid, and configuration [1]. Precisely, different techniques are employed to reduce thermal resistance by generating turbulence in the inner running fluid or increasing the effective surface area. The heat transfer enhancement method can be generally categorized into three classes: active [2,3],

passive [4,5], and compound methods [6]. This is when some external power inputs are either imposed on the fluid or the heated surface so that the rate of heat transfer is enhanced. This issue is somewhat related to the system requirements. Since flow structure analysis is hard to access (owing to external impacts), the methods in this class are deemed complex. Passive methods, on the other hand, take advantage of the modified surfaces and/or insertion of elements, especially turbulence promoters within the flow. Therefore, there is no need to utilize any external power in order to augment the heat transfer. As a result of the alteration of the flow treatment, the coefficient of the convective heat transfer rises. Operating under specific flow and thermal conditions, such techniques come with corresponding pros and cons.

Fin-and-tube heat exchangers (FTHEs) are one of the most widely used heat exchangers for thermal energy conversion and are used in different applications, such as the automotive industry, power plants, electronic devices, process equipment, air conditioning, and refrigeration [7]. Sadeghianjahromi and Wang [7] presented a complete review paper on the previous studies in the field of heat transfer in FTHEs before 2020. The various techniques introduced to improve heat transfer in this type of HE were described in this review paper. Most of these techniques are in the category of passive methods. Recent research in this area is discussed in the following. Gong et al. [8] proposed a new windward Louvered fin structure for use in the fuel cell vehicle radiator. They claimed that due to the airflow deflection, the windward Louvered fin structure significantly improved the thermal performance of the HEs. In addition, Gong et al. [9] proposed the idea of inserting metal elbows into the airside of an FTHE to improve heat transfer in fuel cell vehicles. A comparison between the new structure and the traditional compact radiator was conducted both numerically and experimentally, and a heat transfer improvement of 22% was observed. Altwieb et al. [10] presented a new perforated plain fin structure used for multi-tube, multi-fin heat exchangers. The new fin structure was compared with standard plain and louvered fins. They claimed that by considering both the factors of increasing heat transfer and pressure drop, their proposed fin structure performed better than plain and louvered fin structures. In order to enhance the heat transfer in traditional vehicle radiators, Luo et al. [11] presented three novel structural designs for FTHEs based on wavy-louvered fin and vortex generators. They claimed that these new designs could be used to increase the cooling capability in proton exchange membrane fuel cells. Song et al. [12] suggested a new fin configuration using both concave curved vortex generator pairs and wavy fins in an FTHE. The impact of the concave curved vortex generator pairs location and attack angle on HE performance were investigated numerically. The results showed that adding vortex generators could increase the Nusselt number by 30.6%. Jalil and Goudarzi [13] suggested a nozzle- and diffuser-shaped arrangement of fins to improve the heat transfer in FTHEs. They compared the thermal performance of these two types of fin arrangements with the simple tube. The results revealed that the nozzle-shaped fin structure had a better performance than the other one.

Recently, the passive method of using nanofluids as the working fluid in FTHEs has received much attention. Enhanced heat transfer performance of car radiators is the main purpose of using these nanocoolants. The heat transfer enhancement of using hybrid nanofluids in car radiators was investigated by Li et al. [14]. For this type of FTHE, the maximum convective heat transfer coefficient of the nanocoolant was 26% higher than that of pure ethylene glycol under identical circumstances. A new hybrid nanofluid comprising  $\text{Fe}_2\text{O}_3\text{-TiO}_2$  (50:50) nanoparticles was introduced by Abbas et al. [15]. The nanofluid thermal performance was tested in an aluminum tube automotive radiator for three different nanofluid concentrations. In addition, the impacts of inlet temperature and flow rate were examined. The results showed a large effect of nanoparticle volume fraction on the heat transfer performance of FTHEs. In their experiments, the maximum increase in heat transfer was 26.7%. Xian et al. [16] examined the effect of a hybrid nanocoolant containing carboxyl-functionalized graphene nanoplatelets and titanium dioxide nanoparticles on the thermal performance of an FTHE used in a vehicle cooling system. The results showed

that using a new hybrid nanocoolant led to an increase of up to 35.87% in the overall heat transfer coefficient of the HE in comparison with that using a base coolant.

As an active method, Li et al. [17] introduced a vibration-enhanced heat transfer technology for an FTHE. The vibrations of their experiments had a frequency of 25 kHz and were in the audible range. Their simulations showed that increasing the amplitude and frequency increased the thermal performance of the HE. Furthermore, there are several review papers [18,19] and applied research papers [20–23] dealing with heat transfer enhancement in several types of HEs caused by applying ultrasonic excitation (UE). It should be noted that other methods, such as magnetohydrodynamics (MHD) [24,25], have also been introduced to increase heat transfer in thermal systems.

In this paper, the authors tried to perform a comprehensible study on the effects of UE on heat transfer enhancement of an FTHE experimentally. According to the research literature, the study of UE's effect in this type of HEs is very rare, and much research is needed to prove the efficiency of this technology in this type of exchanger and its commercialization. In fact, most of the proposed techniques for increasing heat transfer in FTHEs have been limited to passive methods, such as modifying the geometry of the fins or substituting the HE operating fluid. Modifying the fin arrangement requires redesigning the existing HEs and in some cases can even increase the structure's weight and pressure drop. Replacing the base fluids, such as water or ethylene glycol, with nanocoolants can also cause the continuous accumulation and sedimentation of nanoparticles in this type of HE, and therefore, its practical implementation is associated with many issues. It is expected that the power UE technology used in the present work, due to its significant effects on the propagation medium, could significantly increase the heat performance of FTHEs.

## 2. Non-Dimensional Numbers and Formulations

Here, some of the most important non-dimensional numbers used in this paper are presented. These dimensionless numbers are defined for the liquid flow inside the tube. First and foremost, the Reynolds ( $Re$ ) number is defined as:

$$Re = \frac{VD_h}{\nu}, \quad (1)$$

where  $\nu = \mu/\rho$  stands for the kinematic viscosity of the fluid, and  $D_h$  is the hydraulic diameter of the tubes.  $\mu$  and  $\rho$  are dynamic viscosity and density, respectively. The Reynolds number for the liquid fluid flow inside the tube varies between 2166 and 6500. In addition, considering the hydraulic diameter of the air conditioning channel as the characteristic length, the air-side Reynolds number will be between 2000 and 9000. The Prandtl ( $Pr$ ) number, the ratio of momentum diffusivity to thermal diffusivity ( $\alpha$ ), is defined as:

$$Pr = \frac{\nu}{\alpha}. \quad (2)$$

The Prandtl number for the water inside the pipes is in the range of  $6.99 < Pr < 9.95$ , and for the flow of air passing over the radiator, it is about 0.7. The Nusselt ( $Nu$ ) number, which plays a critical role in convective heat transfer, is defined as:

$$Nu = \frac{hD_h}{k} \quad (3)$$

where,  $h$  represents the coefficients of the convective heat transfer.  $h$  can also be considered the overall heat transfer coefficient, as follows:

$$h = \frac{q}{A\Delta T_{bulk}}. \quad (4)$$

where  $q = \rho Q c_p (T_i - T_o)$  is the heat transfer rate, and this can be calculated by means of the energy balance equation. The temperatures of the liquid flowing inside the tube at the inlet and outlet of the FTHE are shown via  $T_i$  and  $T_o$ , respectively.  $c_p$  denotes the thermal capacity of the liquid and is calculated at the bulk temperature of the liquid fluid flow.  $Q$  is the volumetric flow rate recorded by the flow meter (Figure 1). In addition,  $A$  is the peripheral area of the tube that is in contact with water and can be calculated by the following equation:

$$A = 2(lw + lH) \tag{5}$$

where  $l$ ,  $w$ , and  $H$  are the length, width, and height of the tube which are shown in Figure 2.

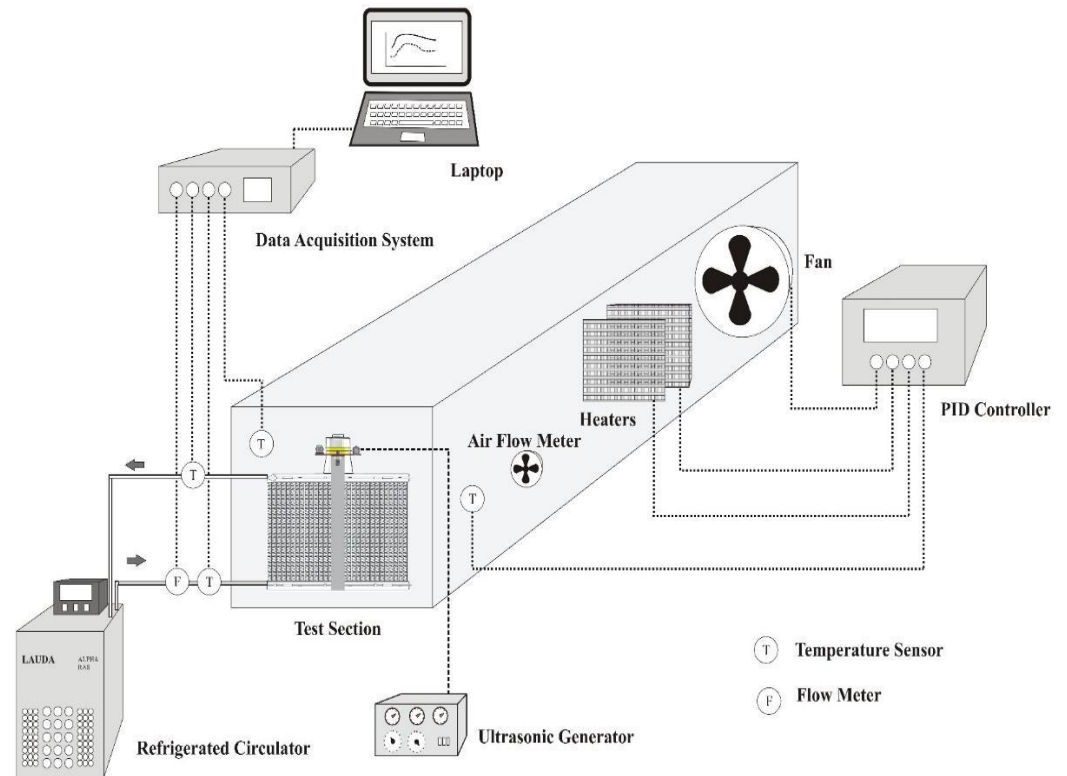


Figure 1. The schematic of the experimental setup.

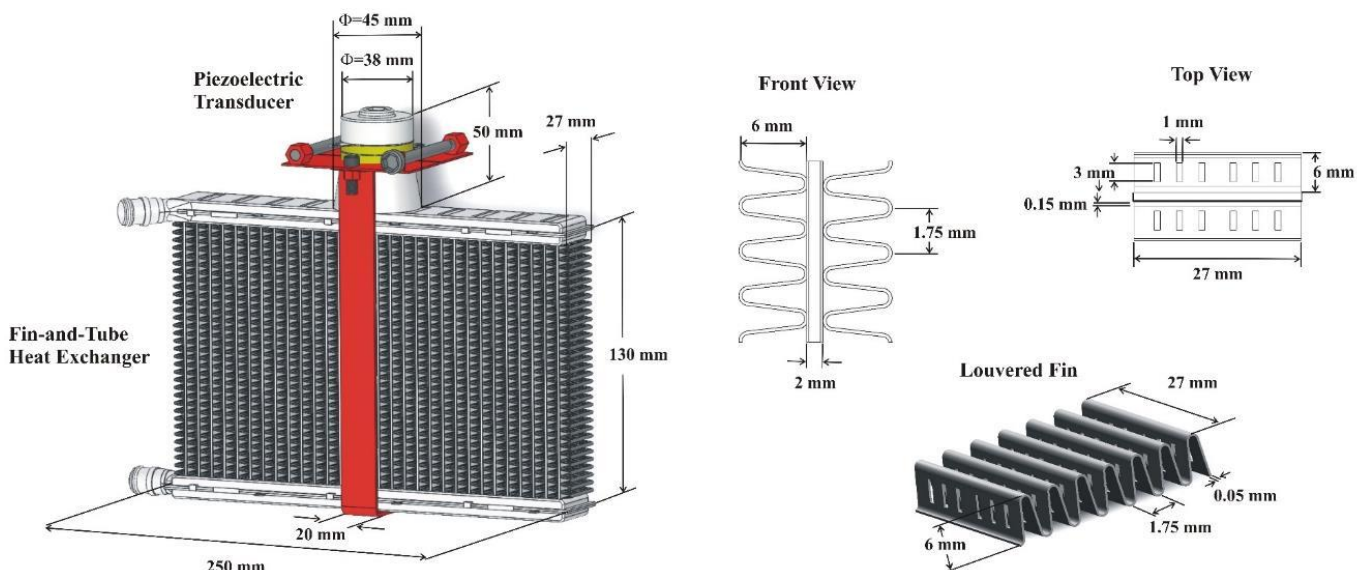


Figure 2. The schematic of the fin-and-tube heat exchanger, piezoelectric transducer, and louvered fin.

Moreover,  $\Delta T_{bulk}$  is the difference between the bulk temperature of the fluid flow inside the test section and the wall temperature ( $T_w$ ). Using the mean temperature method,  $\Delta T_{bulk}$  is calculated as [26]:

$$\Delta T_{bulk} = \left( \frac{T_i + T_o}{2} \right) - T_w \quad (6)$$

### 3. Methodology

Here, the experimental apparatus, setup, and methods of gathering results are presented and discussed. To study the impacts of UE on the heat transfer rate, an experimental apparatus was constructed. The schematic of the apparatus and instrumentation of the experiment are depicted in Figure 1. This system was actually an upgraded air conditioning testing system that included an air conditioning tunnel with dimensions of 200 (cm)  $\times$  35 (cm)  $\times$  35 (cm). The air conditioning tunnel was equipped with a blower fan with remote control capability with an accuracy of 1 (RPM), which allowed testing for different air flows. Two heaters (PTFE) with a power range of 0–3500 (W) were located in the air channel to control the temperature of the air over the test section. These heaters used PID control to adjust the desired air temperature. Four temperature sensors (Maxim Integrated Co., Accuracy:  $\pm 0.5$  ( $^{\circ}\text{C}$ )) were used. Two of them were located at the inlet and outlet of the FTHE to measure the liquid inlet and outlet temperatures, which changed in the range of 12 ( $^{\circ}\text{C}$ ) to 20 ( $^{\circ}\text{C}$ ). The other temperature sensors were used to detect the air passing temperatures ranging between 25 ( $^{\circ}\text{C}$ ) to 45 ( $^{\circ}\text{C}$ ). An airflow meter (Testo 400, Range: 0–10 (m/s), Accuracy:  $\pm 0.04$  (m/s)) was utilized to measure the air passing velocity over the FTHE, which varied between 0.1 (m/s) to 4 (m/s). A refrigerated circulator (Lauda, Alpha R8) equipped with affordable cooling thermostats and a heating unit with the ability to maintain temperatures from  $-25$  to 100 ( $^{\circ}\text{C}$ ) (in the lab) was used to supply water with the desired temperature and flow rate to the entrance of the test section. A flow meter (Nixon Flow Meter LTD Co, Model: NT5, Range 1.2–10 (L/min), Accuracy:  $\pm 5\%$ ) was used to record the volumetric flow rate of the liquid flow in the radiator. In the current experimental tests, the liquid flow rate was in the range of 2 to 6 (L/min).

A radiator (250  $\times$  130 (mm)) made of aluminum alloy was considered the FTHE. A 40 (kHz) ultrasonic transducer (Hesentec Ultrasonic Co., Model: HS-8SH-3840) was powered by an ultrasonic generator (Hesentec Ultrasonic Co., Ultrasonic PCB Driver Ultrasonic Generator) with a power level of 50 (W). Two data types were obtained for each test case, one with the presence of ultrasonic excitation and the other in the silent state (no vibration), and then the obtained data were compared. As for recording data, all sensors were connected to a handheld control unit. This unit had the ability to send all the information obtained to the computer for further analysis. Furthermore, detailed drawings of the FTHE, piezoelectric transducer, and louvered fin are presented in Figure 2. As shown in Figure 2, a metal belt (in red) with a width of 20 mm and a thickness of 3 mm was used to mount the piezoelectric transducer. The piezoelectric transducer was connected to this adjustable structure by several screws on the top of FTHE, and its lower surface was exactly tangential to the FTHE to ensure the transmission of UE to the radiator. The Moffat method [27] was used to calculate the uncertainty of the experiments. Using this method, the uncertainty values of the Reynolds number, Nusselt number, and heat transfer rate were  $\pm 5\%$ ,  $\pm 3.4\%$ , and  $\pm 2.6\%$ , respectively. It should be noted that the assumptions of (1) constant ambient air temperature and (2) equal wall temperature between the outer surface of the radiator's tube and its inner surface (due to very low thickness) were considered in the theoretical analysis of the present work.

### 4. Results and Discussions

In this section, the thermal effect of UE in the FTHEs is discussed. Then, the validity of the obtained data is checked, and at the end, the thermal findings are presented and discussed in detail.

#### 4.1. Validation

For validation, the authors took advantage of the empirical correlation reported by Dittus-Boelter [28]. The Dittus-Boelter correlation is expressed via the non-dimensional parameters of  $Re$  and  $Pr$ , as follows:

$$Nu = 0.023 Re^{0.8} Pr^n \quad (7)$$

where  $n$  equals 0.4 and 0.3 for heating and cooling, respectively. The variation of the  $Nu$  number at different Reynolds numbers ranging from 2000 to 7000 is compared and presented in Table 1. Additionally, the percentage differences (Errors) between the current results and those of Dittus-Boelter [28] are mentioned in Table 1. As can be seen, there was a close match between the trend and data and that of Dittus-Boelter [28], which ensures the validity of the findings as well as the reliability of the facility.

**Table 1.** Comparison of the Nusselt numbers that resulted from the current research with those of the Dittus-Boelter correlation [28].

	Current Research	Dittus-Boelter Correlation	Error (%)
$Re = 2166$	10.47	9.16	14.30%
$Re = 4333$	17.01	15.95	6.64%
$Re = 6500$	22.29	22.06	1.04%

#### 4.2. The Effect of UE on the Outlet Temperature

In this section, the outlet temperature is studied in a very comprehensive way. To do so, various  $Re$  numbers ranging from 2166 to 6500 for the water flowing into the test section were considered. Four different velocities ( $U = 0.1, 0.5, 1,$  and  $4 \left(\frac{m}{s}\right)$ ) for the air passing through the FTHE were also taken into account, and  $T_\infty$  varied from 25 ( $^\circ C$ ) to 45 ( $^\circ C$ ). Figures 3–6, which show the variation of the outlet temperature against  $Re$  number, are presented to examine the presence of the ultrasonic field. Furthermore, the variation percentage is calculated and shown in the figures. All figures are presented in the absence of vibrations ( $UP = 0$ ) and the presence of ultrasonic excitation with a power level of 50 Watts ( $UP = 50$  (W)).

Increasing the ambient temperature with constant Reynolds numbers raised the wall temperature of the radiator tube and thus increased  $\Delta T_{bulk}$ . As a result, the heat transfer rate to the radiator increased, and the outlet fluid temperature grew. In addition, growing the velocity of the air passing over the radiator ( $U$ ) increased the heat transfer coefficient and consequently increased the heat transfer rate. However, on the other hand, with an increasing velocity of liquid flow inside the tubes and an increasing mass flow, the rate of temperature change of the outlet liquid fluid flow was less (Figures 3–6). In the following, we focus more on the effects of ultrasonic excitation.

As can be seen, there was a consistent trend among the data, and as expected, with an increase in the  $Re$  number, the impact of UE on the outlet temperature generally faded (in all values of air passing velocity as well as ambient temperature). Accordingly, at lower air passing velocities as well as lower ambient temperatures, the influence of the vibration was highlighted more. However, with increases in  $T_\infty$  and  $U$ , the mentioned effects decreased. The most sensible effects on the outlet temperature (with 9.14%) could be seen when  $U$  and  $T_\infty$  are equal to  $0.1 \left(\frac{m}{s}\right)$  and 25 ( $^\circ C$ ), respectively. This can be attributed to the formation of micro-bubbles and their collision within a liquid due to acoustic excitation [29]. Increasing the ambient temperature (at a constant  $Re$ ) raised the water temperature inside the tubes. As the water temperature increased, the solubility of the air in the water decreased [30], resulting in a lower rate of microbubble formation. Therefore, as mentioned, the effect of ultrasound was reduced.

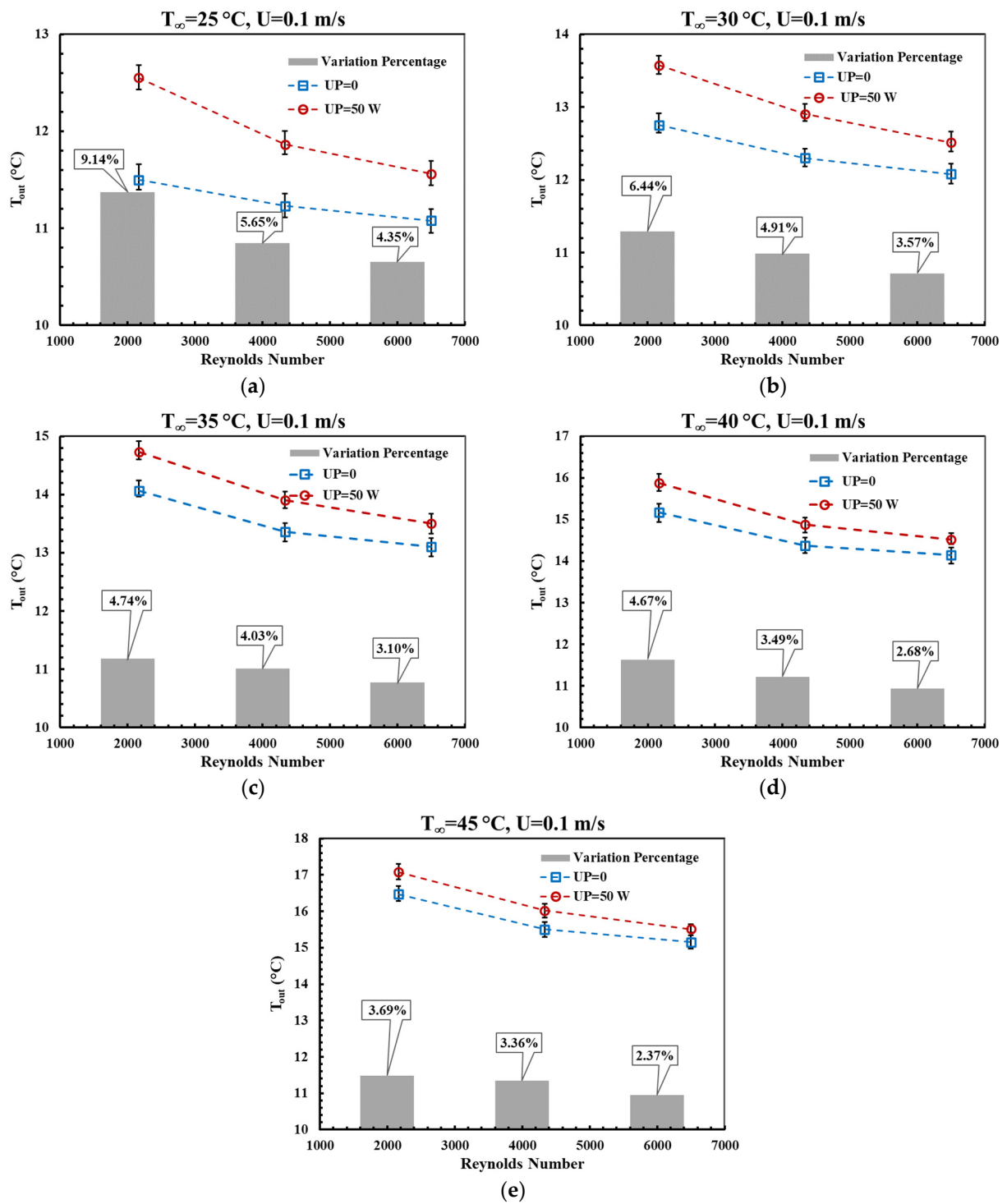
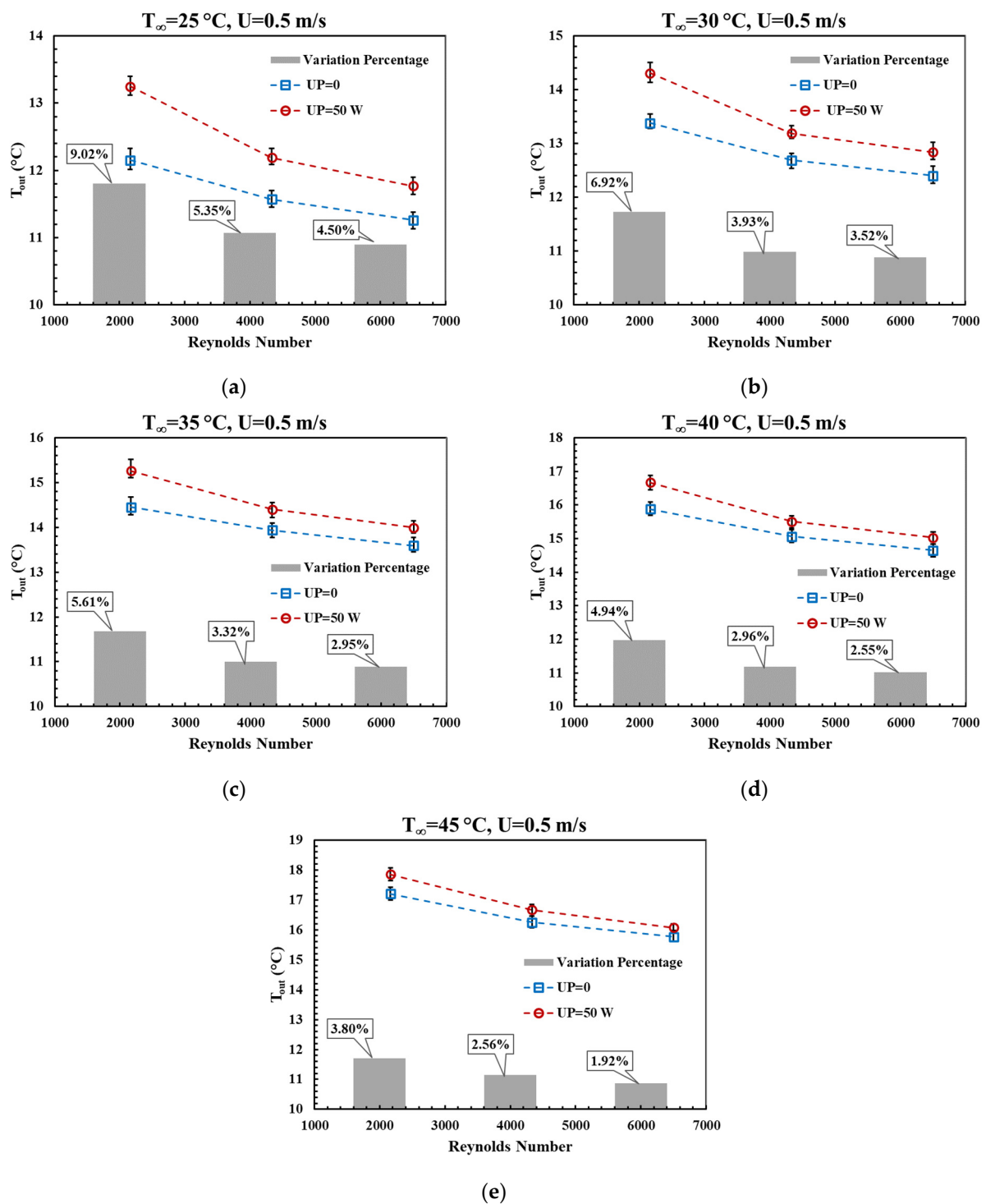
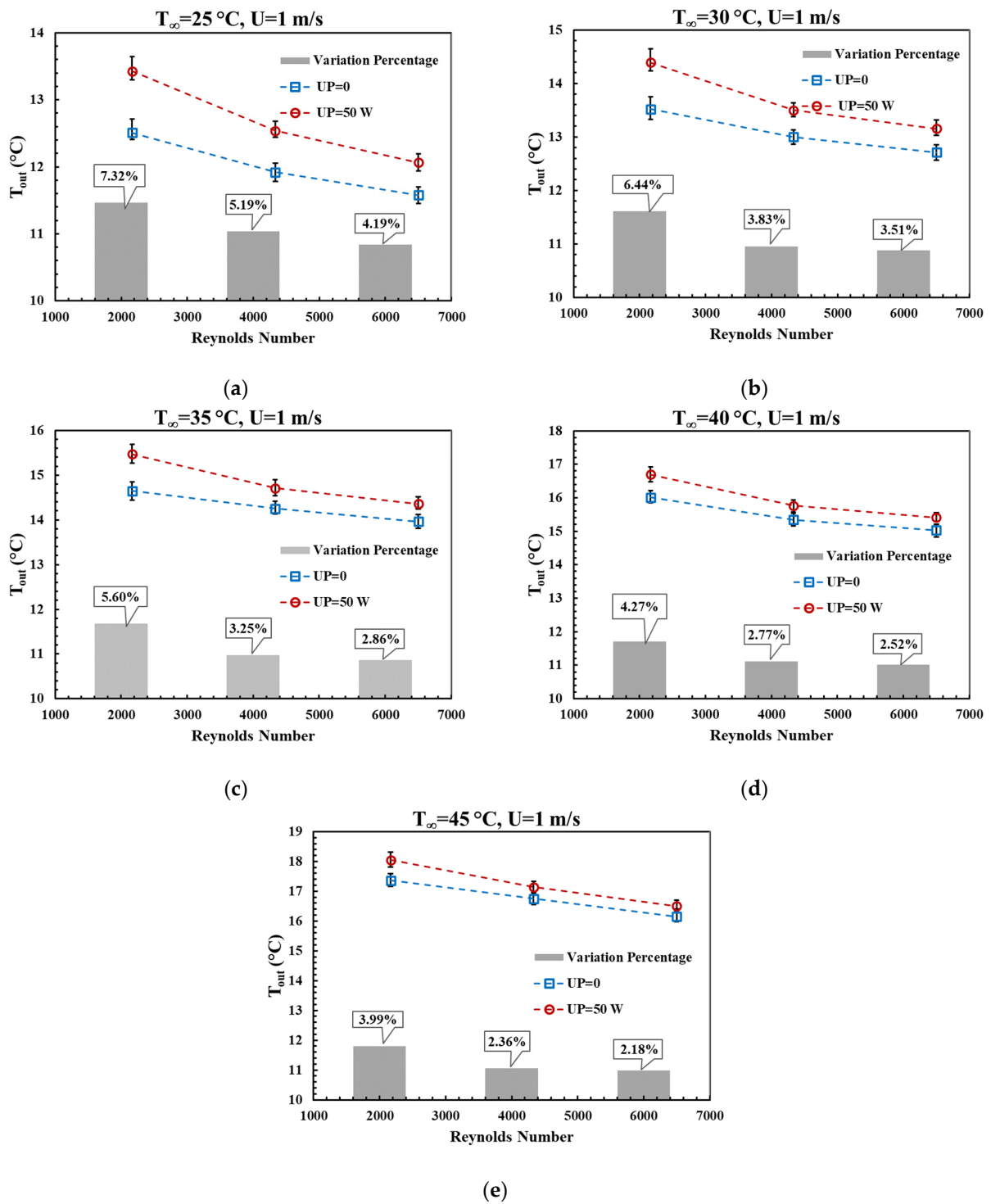


Figure 3. Variation of outlet temperature versus Re number at  $U = 0.1$  ( $\frac{m}{s}$ ) and (a)  $T_{\infty} = 25$  (°C), (b)  $T_{\infty} = 30$  (°C), (c)  $T_{\infty} = 35$  (°C), (d)  $T_{\infty} = 40$  (°C), and (e)  $T_{\infty} = 45$  (°C). The results are presented in a no-vibration state (UP = 0) and in the presence of vibration with ultrasonic power of 50 Watts (UP = 50 (W)).



**Figure 4.** Variation of outlet temperature versus Re number at  $U = 0.5$  ( $\frac{m}{s}$ ) and (a)  $T_{\infty} = 25$  (°C), (b)  $T_{\infty} = 30$  (°C), (c)  $T_{\infty} = 35$  (°C), (d)  $T_{\infty} = 40$  (°C), and (e)  $T_{\infty} = 45$  (°C). The results are presented in a no-vibration state (UP = 0) and in the presence of vibration with ultrasonic power of 50 Watts (UP = 50 (W)).



**Figure 5.** Variation of outlet temperature versus Re number at  $U = 1$  ( $\frac{m}{s}$ ) and (a)  $T_{\infty} = 25$  (°C), (b)  $T_{\infty} = 30$  (°C), (c)  $T_{\infty} = 35$  (°C), (d)  $T_{\infty} = 40$  (°C), and (e)  $T_{\infty} = 45$  (°C). The results are presented in a no-vibration state (UP = 0) and in the presence of vibration with ultrasonic power of 50 Watts (UP = 50 (W)).

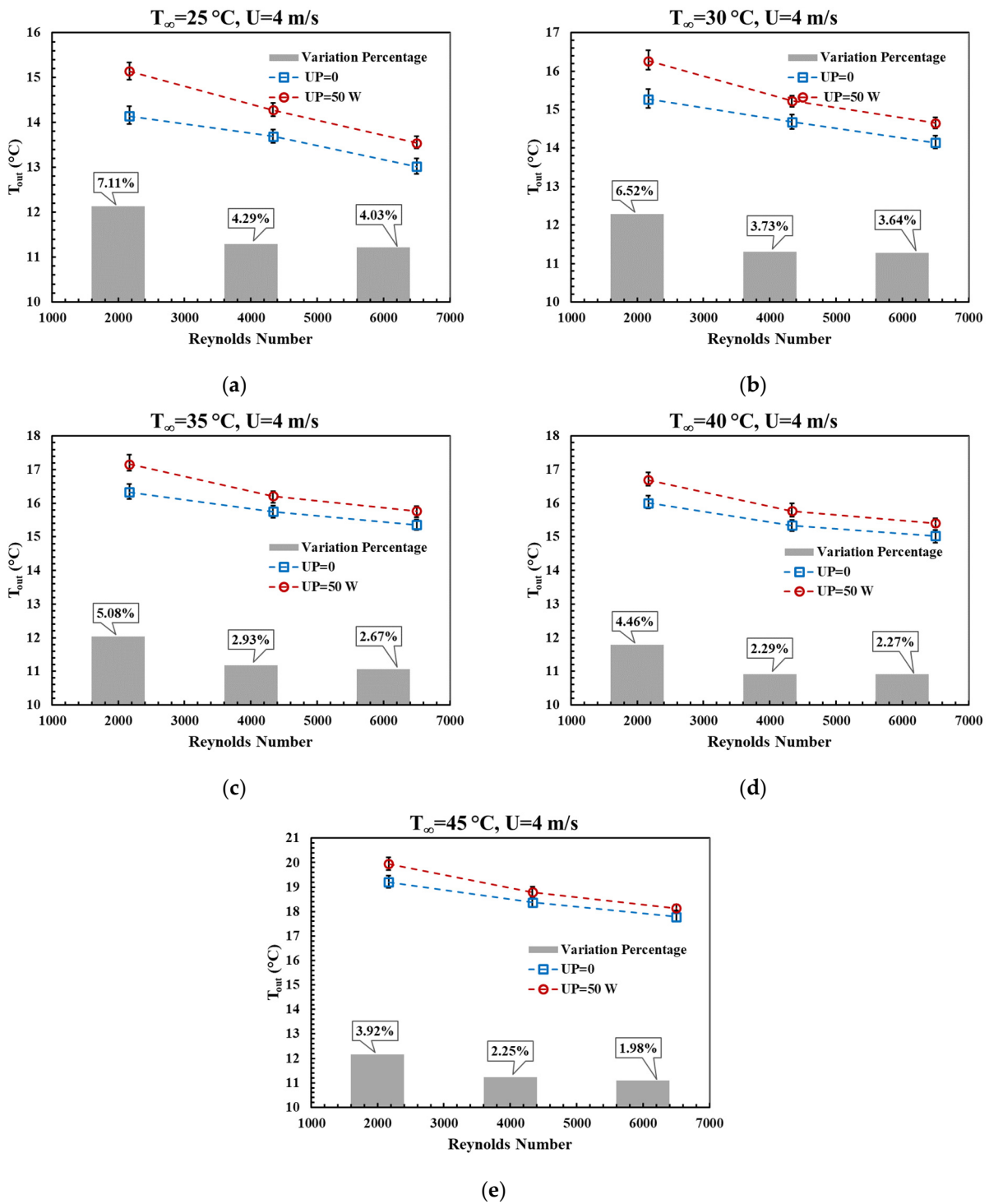


**Figure 6.** Variation of outlet temperature versus Re number at  $U = 4$  (m/s) and (a)  $T_{\infty} = 25$  (°C), (b)  $T_{\infty} = 30$  (°C), (c)  $T_{\infty} = 35$  (°C), (d)  $T_{\infty} = 40$  (°C), and (e)  $T_{\infty} = 45$  (°C). The results are presented in a no-vibration state (UP=0) and in the presence of vibration with ultrasonic power of 50 Watts (UP = 50 (W)).

#### 4.3. The Effect of UE on Heat Flow

Here, the heat convection to the fluid in the FTHE under the influence of UE is studied in detail. For this test, the ambient temperature ranged from 25 (°C) to 45 (°C), and four different velocities ( $U = 0.1, 0.5, 1,$  and  $4$  ( $\frac{m}{s}$ )) for the air passing through the FTHE were considered. Additionally, the Reynolds number (Re) effect was taken into account and

examined for three values: 2166, 4333, and 6500. Figures 7–10, which show the variation in heat flow against ambient temperature, are presented to examine the presence of the acoustic field and state the variation percentage. As can be seen in the figures, there was a general increase in the heat flow in comparison to the case in which there was no acoustic vibration. As expected, apart from the influence of UE, the exchanged heat flow increased as the ambient temperature rose. This was because of the increase in the temperature difference between the medium fluid and that of the surroundings. It was also found that the impact of UE lessened as the ambient temperature increased, especially at a higher  $Re$  and  $U$ . As a result of this, the amount of transferred heat flow dropped.

In the current test, considering various discussed parameters, UE had the strongest influence on heat flow (70.11%) when  $Re = 2166$  and  $T_{\infty} = 25$  (°C). On the other hand, the lowest (9.31%) was associated with the case in which  $Re = 6500$  and  $T_{\infty} = 45$  (°C).

#### 4.4. The Impact of UE on Nusselt Number

As shown in Figures 11–15, the current test focused on the impact of UE on the Nusselt number, and the figures show its variation against  $U$ . The test covered the ranges of  $Re = 2166$  to 6500 and  $T_{\infty} = 25$  to 45 (°C), and  $U = 0.1$  to 4 ( $\frac{m}{s}$ ).

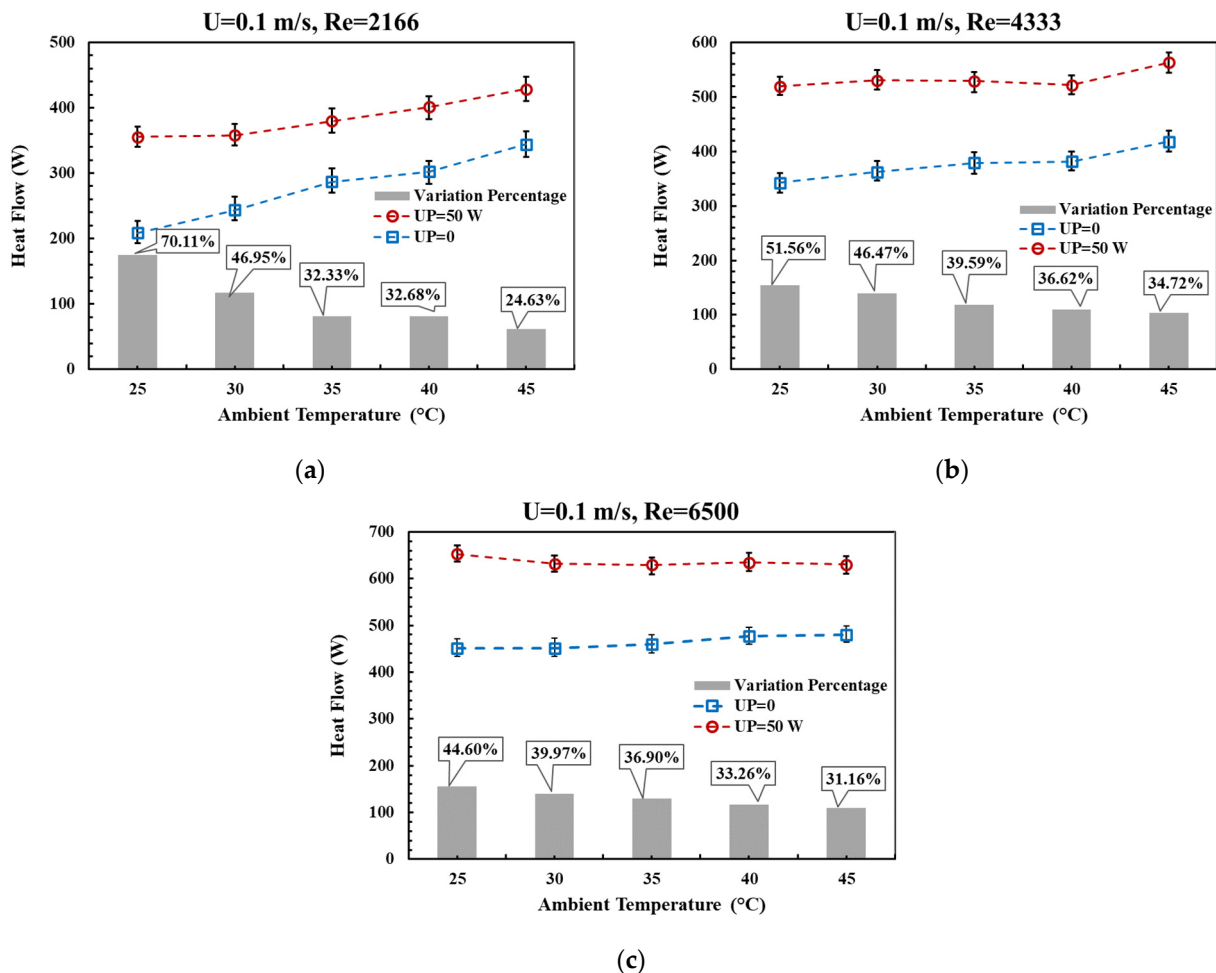


**Figure 7.** The variations of heat flow against ambient temperature at  $U = 0.1$  (m/s) and Reynolds numbers of (a)  $Re = 2166$ , (b)  $Re = 4333$ , (c)  $Re = 6500$ . The results are presented in a no-vibration state ( $UP = 0$ ) and in the presence of vibration with ultrasonic power of 50 Watts ( $UP = 50$  (W)).

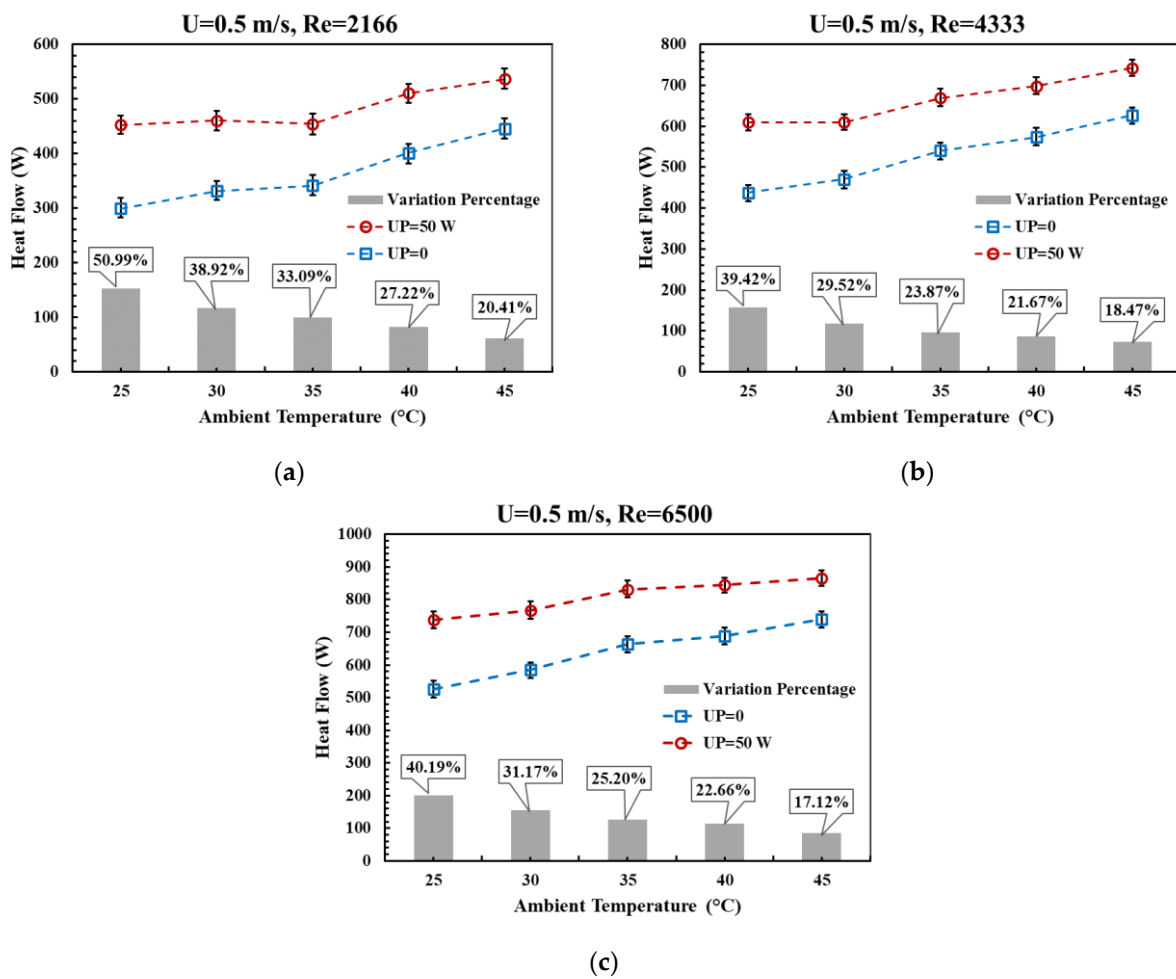


**Figure 8.** The variations of heat flow against ambient temperature at  $U = 0.5$  (m/s) and Reynolds numbers of (a)  $Re = 2166$ , (b)  $Re = 4333$ , and (c)  $Re = 6500$ . The results are presented in a no-vibration state ( $UP = 0$ ) and in the presence of vibration with ultrasonic power of 50 Watts ( $UP = 50$  W).

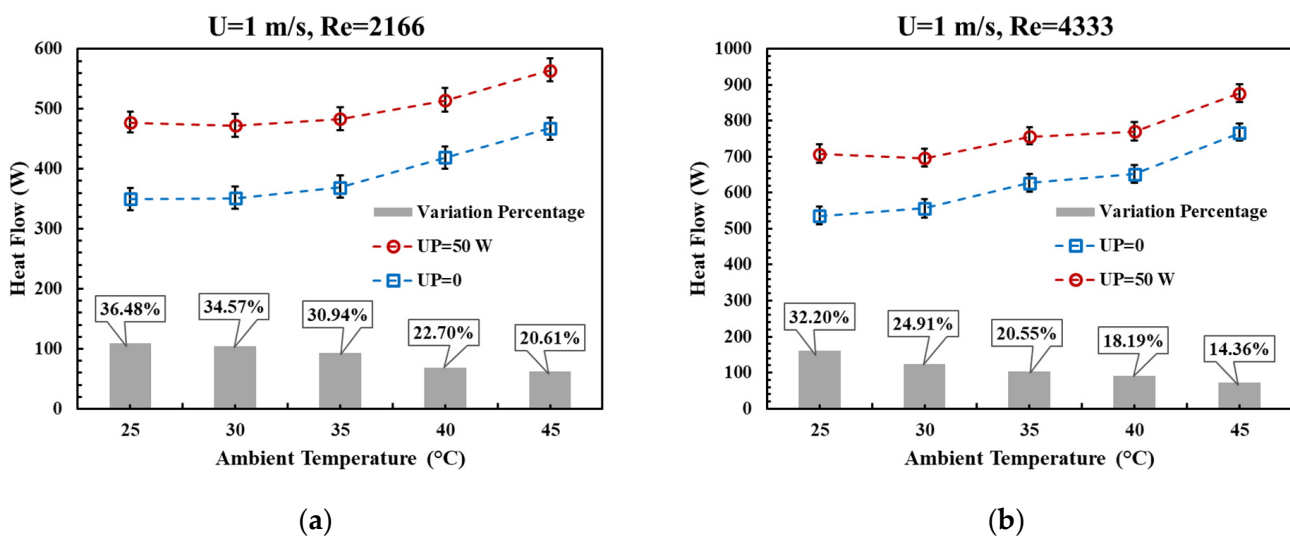
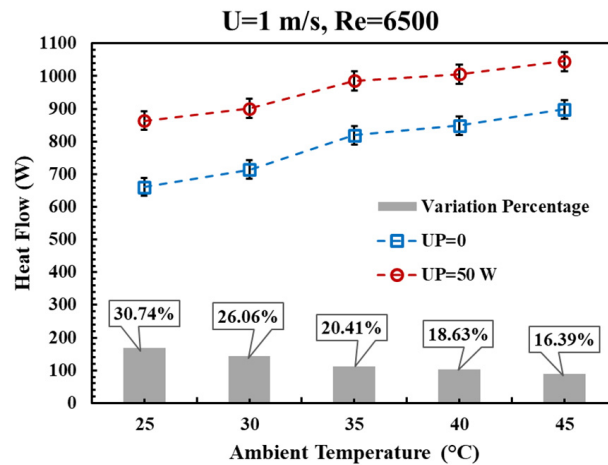
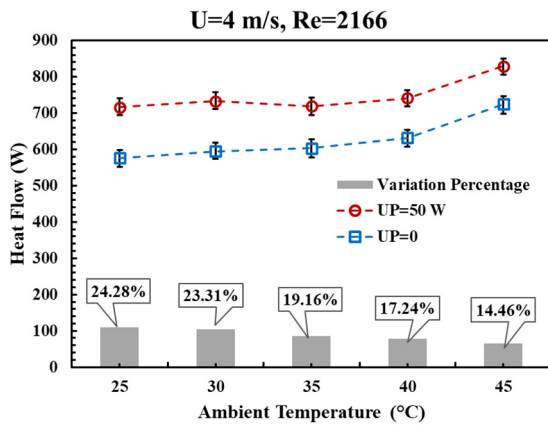


**Figure 9.** Cont.

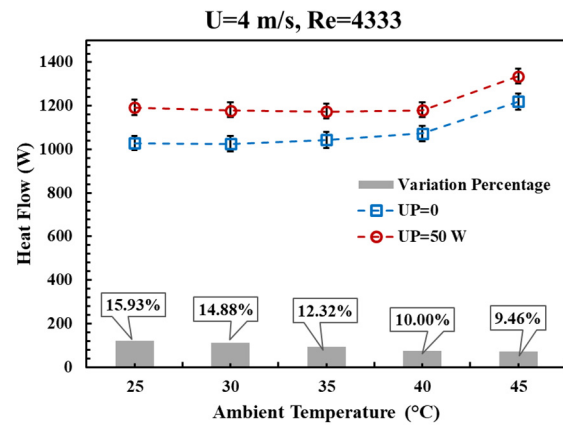


(c)

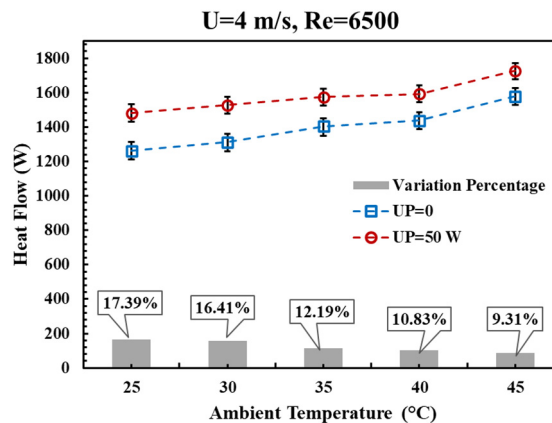
**Figure 9.** The variations of heat flow against ambient temperature at  $U = 1$  (m/s) and Reynolds numbers of (a)  $Re = 2166$ , (b)  $Re = 4333$ , and (c)  $Re = 6500$ . The results are presented in a no-vibration state ( $UP = 0$ ) and in the presence of vibration with ultrasonic power of 50 Watts ( $UP = 50$  (W)).



(a)



(b)



(c)

**Figure 10.** The variations of heat flow against ambient temperature at  $U = 4$  (m/s) and Reynolds number of (a)  $Re = 2166$ , (b)  $Re = 4333$ , (c)  $Re = 6500$ . The results are presented in no vibration state ( $UP = 0$ ) and in the presence of vibration with ultrasonic power of 50 Watts ( $UP = 50$  (W)).

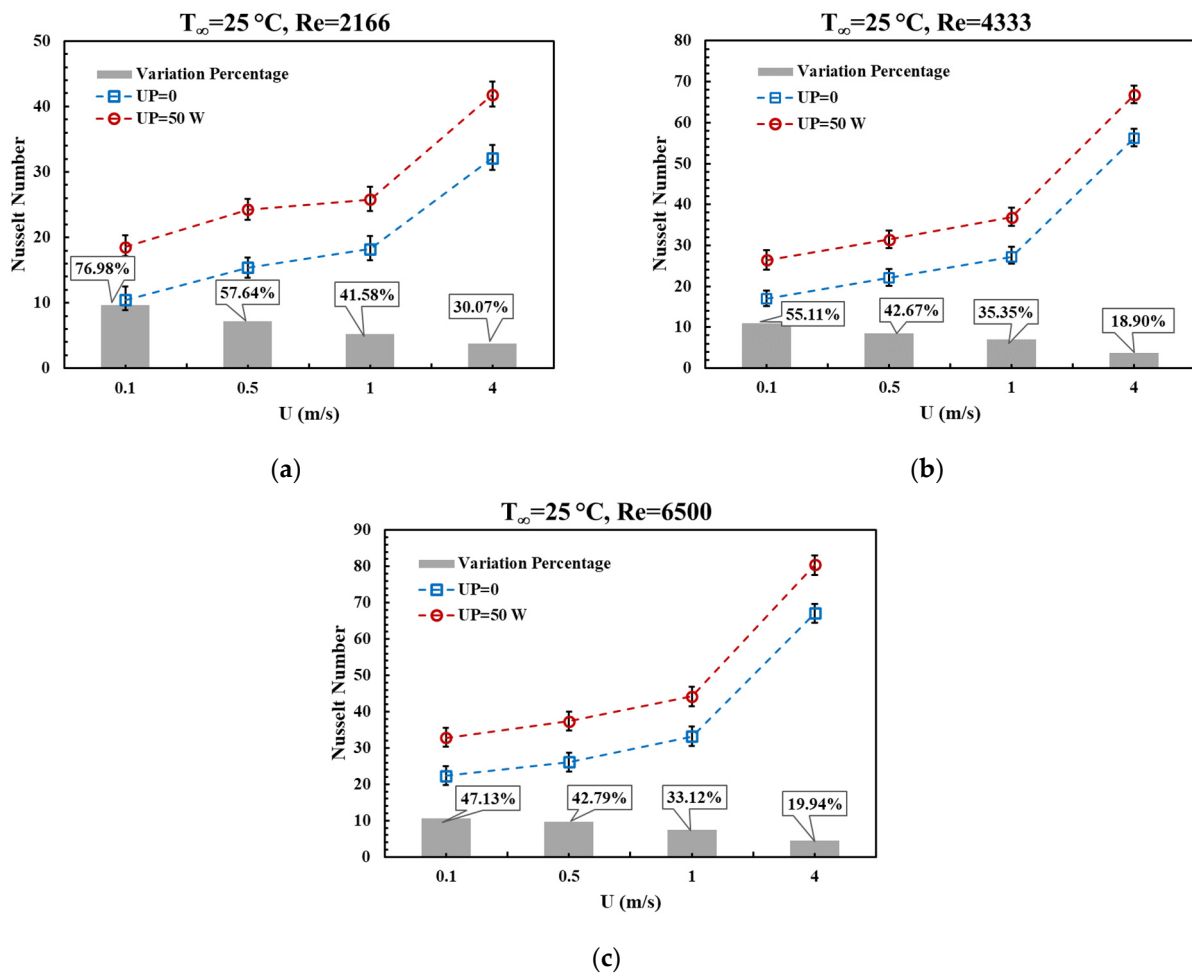


**Figure 11.** The variations of Nusselt number against  $U$  at  $T_{\infty} = 25^{\circ}\text{C}$  and Reynolds numbers of (a)  $Re = 2166$ , (b)  $Re = 4333$ , and (c)  $Re = 6500$ . The results are presented in a no-vibration state ( $UP = 0$ ) and in the presence of vibration with ultrasonic power of 50 Watts ( $UP = 50\text{ W}$ ).

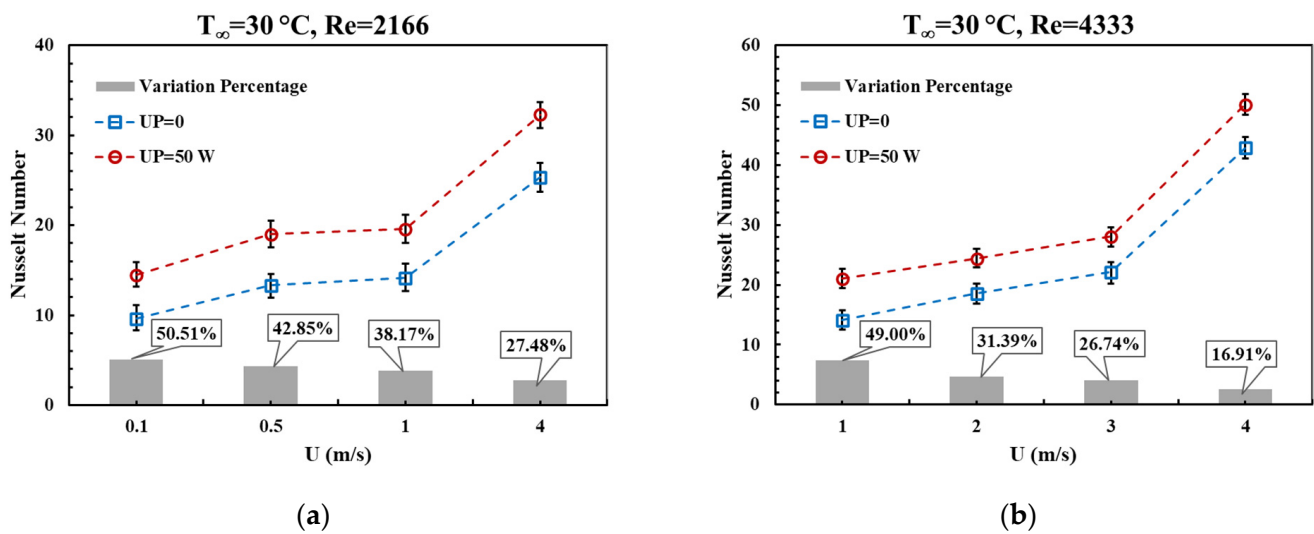
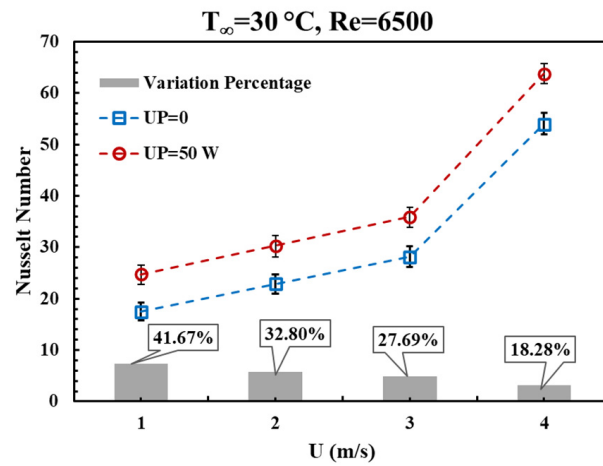
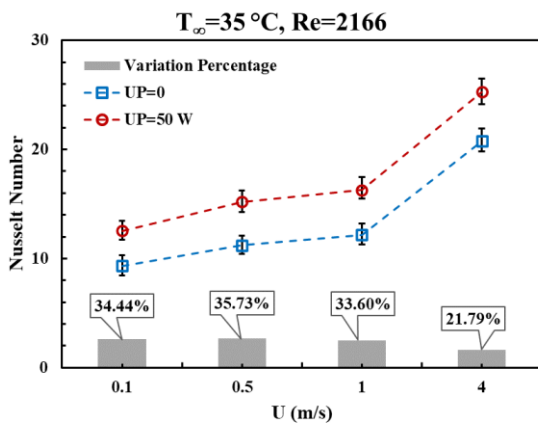


**Figure 12. Cont.**

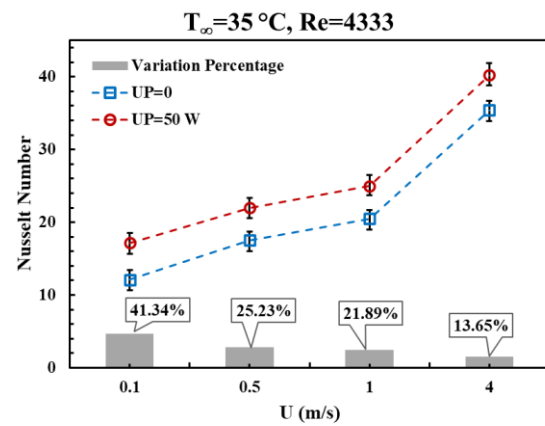


(c)

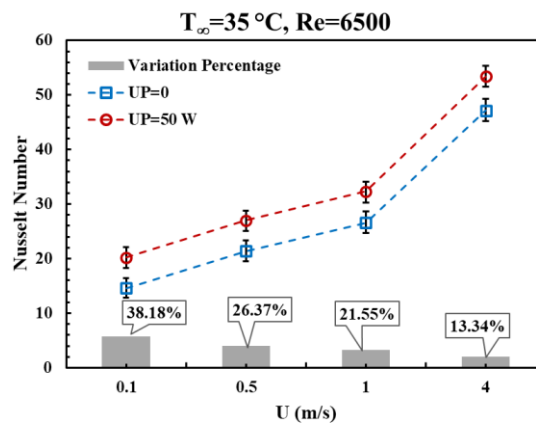
**Figure 12.** The variations of Nusselt number against  $U$  at  $T_{\infty} = 30$  ( $^{\circ}\text{C}$ ) and Reynolds numbers of (a)  $Re = 2166$ , (b)  $Re = 4333$ , and (c)  $Re = 6500$ . The results are presented in a no-vibration state ( $UP = 0$ ) and in the presence of vibration with ultrasonic power of 50 Watts ( $UP = 50$  (W)).



(a)



(b)



(c)

**Figure 13.** The variations of Nusselt number against  $U$  at  $T_{\infty} = 35$  ( $^{\circ}\text{C}$ ) and Reynolds numbers of (a)  $Re = 2166$ , (b)  $Re = 4333$ , and (c)  $Re = 6500$ . The results are presented in a no-vibration state ( $UP = 0$ ) and in the presence of vibration with ultrasonic power of 50 Watts ( $UP = 50$  (W)).

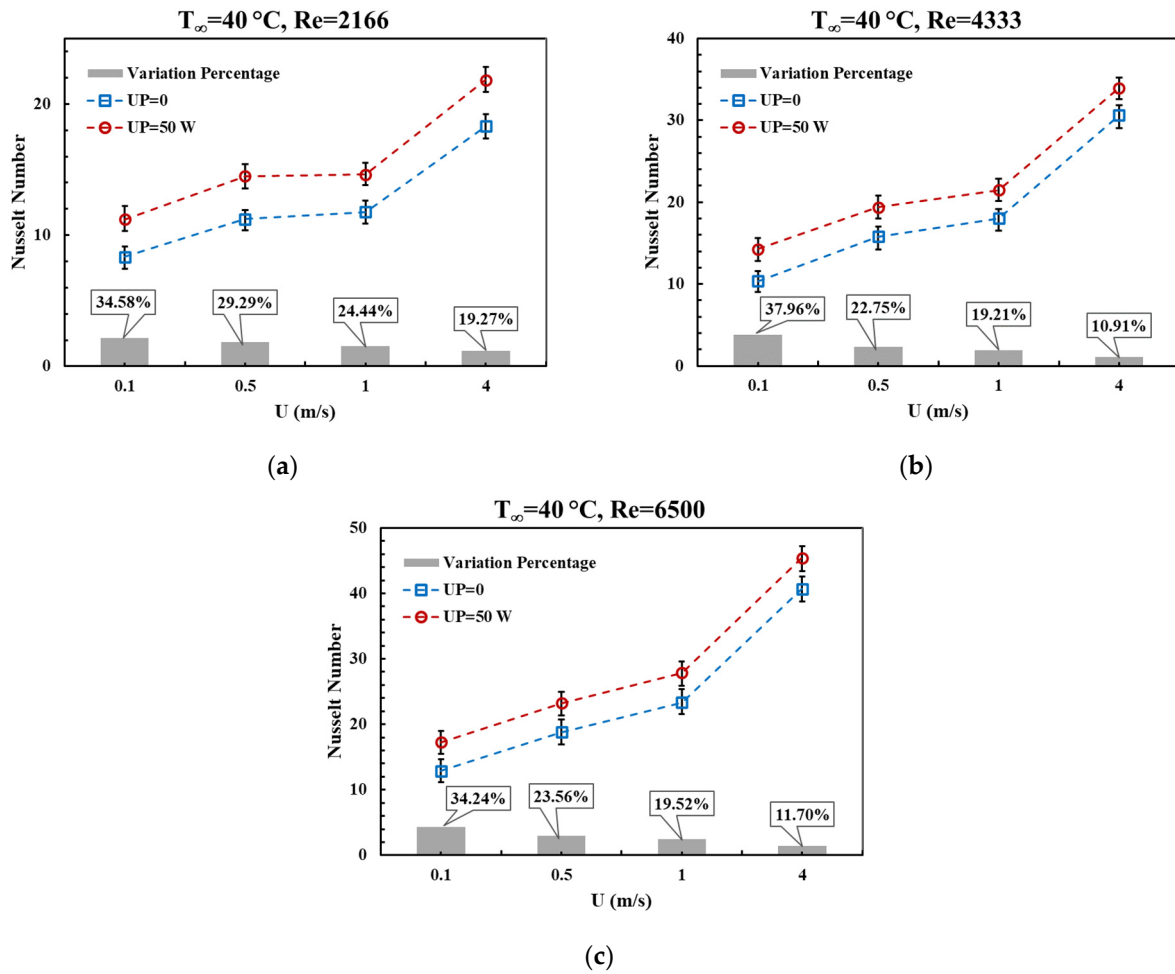


**Figure 14.** The variations of Nusselt number against  $U$  at  $T_{\infty} = 40$  ( $^{\circ}\text{C}$ ) and Reynolds numbers of (a)  $Re = 2166$ , (b)  $Re = 4333$ , and (c)  $Re = 6500$ . The results are presented in a no-vibration state ( $UP = 0$ ) and in the presence of vibration with ultrasonic power of 50 Watts ( $UP = 50$  (W)).

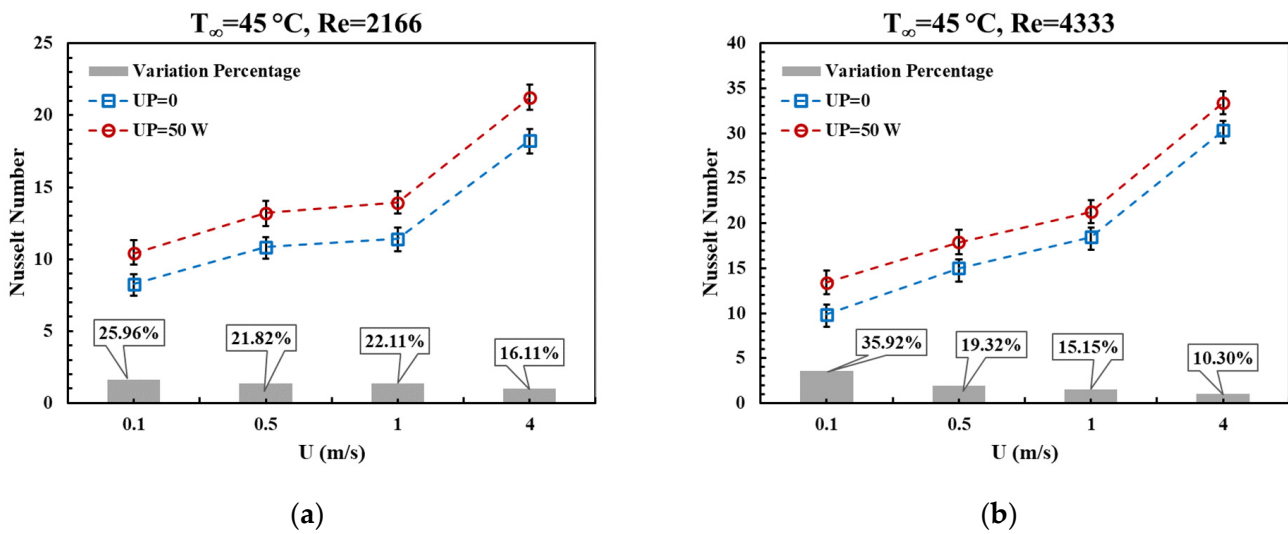
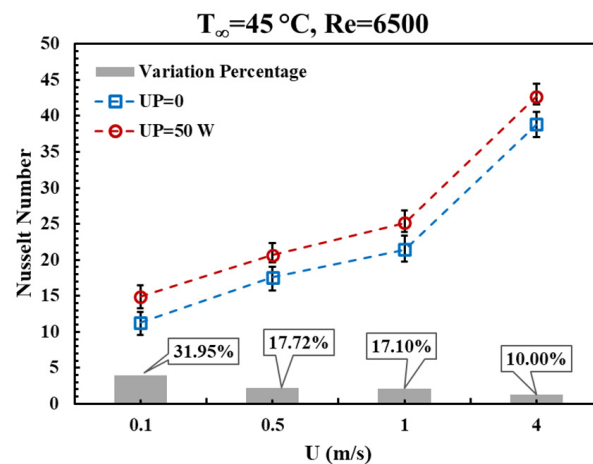


**Figure 15.** Cont.



(c)

**Figure 15.** The variations of Nusselt number against  $U$  at  $T_{\infty} = 45$  ( $^{\circ}\text{C}$ ) and Reynolds numbers of (a)  $Re = 2166$ , (b)  $Re = 4333$ , and (c)  $Re = 6500$ . The results are presented in a no-vibration state ( $UP = 0$ ) and in the presence of vibration with ultrasonic power of 50 Watts ( $UP = 50$  (W)).

As can be seen, the  $Nu$  number, regardless of the presence of UE, increased as  $U$  increased, and this was because an enhancement in the velocity led to an increase in the coefficient of convection heat transfer. As ultrasonic was imposed on the test case, there was an overall enhancement in the variations of the Nusselt number. To be precise, the impact of UE was more dominant when the case was operating at a lower  $U$ s. The most significant case was when  $Re = 2166$  and  $T_{\infty} = 25$  ( $^{\circ}\text{C}$ ), and in this case, the variation percentage was 76.98%, while the least (with 10%) was when  $Re = 6500$  and  $T_{\infty} = 45$  ( $^{\circ}\text{C}$ ). Furthermore, at a lower  $U$ s, the vibration could significantly affect the mixture of the boundary layers on the fins.

## 5. Conclusions

In the current experimental study, an attempt was made to study the effects of ultrasonic excitation on the rate of convection heat transfer in a louvered FTHE. An experimental system was designed and made to help understand the influence of various engineering parameters, such as the air passing velocity, ambient temperature, Nusselt number, and Reynolds number. The findings can be expressed as follows:

It was found that enhancing the flow rate had a negative effect on the UE's impact on heat transfer enhancement in this type of HE.

Increasing the velocity of the air passing over the HE generally increased heat transfer; however, it undermined the presence of ultrasonic excitation.

With an increase in the surrounding temperature, the temperature difference between the running water and air passing the fins increased, and this also adversely affected the ultrasonic excitation's imposition.

In the current experimental conditions, the highest increase in heat transfer was equal to 70.11%, recorded with  $Re = 2166$ , an ambient temperature of  $25$   $^{\circ}\text{C}$ , and an air velocity of  $0.1$  m/s.

It should be noted that ultrasonic excitation, in addition to improving heat transfer, can also result in the continuous cleaning of equipment and a reduction in maintenance costs.

**Author Contributions:** A.A.D.: Conceptualization, Methodology, Writing—Original Draft; H.S.: Formal Analysis, Investigation; M.A.: Formal Analysis, Investigation, M.H.: Investigation, Data Curation; M.B.B.H.: Software, Validation; A.A.: Formal Analysis, Investigation. All authors have read and agreed to the published version of the manuscript.

**Funding:** This work was supported by the Iran National Science Foundation (INSF), INSF, Iran (grant number: 98000177).

**Data Availability Statement:** All data generated or analyzed during this study are included in this published article.

**Acknowledgments:** The authors sincerely thank the editors and the reviewers for their valuable comments and suggestions, which greatly improve the quality of this article.

**Conflicts of Interest:** All authors declare that they have no conflict of interest.

## References

1. Alam, T.; Kim, M.H. A comprehensive review on single phase heat transfer enhancement techniques in heat exchanger applications. *Renew. Sustain. Energy Rev.* **2018**, *81*, 813–839. [[CrossRef](#)]
2. Wang, J.; Fu, R.; Hu, X. Experimental study on EHD heat transfer enhancement with a wire electrode between two divergent fins. *Appl. Therm. Eng.* **2019**, *148*, 457–465. [[CrossRef](#)]
3. Bezaatpour, M.; Goharkah, M. Convective heat transfer enhancement in a double pipe mini heat exchanger by magnetic field induced swirling flow. *Appl. Therm. Eng.* **2020**, *167*, 114801. [[CrossRef](#)]
4. Li, X.; Zhu, D.; Sun, J.; Mo, X.; Yin, Y. Air side heat transfer and pressure drop of H type fin and tube bundles with in line layouts. *Exp. Therm. Fluid Sci.* **2018**, *96*, 146–153. [[CrossRef](#)]
5. Bhanvase, B.; Sayankar, S.; Kapre, A.; Fule, P.; Sonawane, S. Experimental investigation on intensified convective heat transfer coefficient of water based PANI nanofluid in vertical helical coiled heat exchanger. *Appl. Therm. Eng.* **2018**, *128*, 134–140. [[CrossRef](#)]
6. Alamgholilou, A.; Esmailzadeh, E. Experimental investigation on hydrodynamics and heat transfer of fluid flow into channel for cooling of rectangular ribs by passive and EHD active enhancement methods. *Exp. Therm. Fluid Sci.* **2012**, *38*, 61–73. [[CrossRef](#)]
7. Sadeghianjahromi, A.; Wang, C.C. Heat transfer enhancement in fin-and-tube heat exchangers—A review on different mechanisms. *Renew. Sustain. Energy Rev.* **2021**, *137*, 110470. [[CrossRef](#)]
8. Gong, C.; Shen, J.; Yu, Y.; Wang, K.; Tu, Z. A novel radiator structure for enhanced heat transfer used in PEM fuel cell vehicle. *Int. J. Heat Mass Transf.* **2020**, *157*, 119926. [[CrossRef](#)]
9. Gong, C.; Du, Y.; Yu, Y.; Chang, H.; Luo, X.; Tu, Z. Numerical and experimental investigation of enhanced heat transfer radiator through air deflection used in fuel cell vehicles. *Int. J. Heat Mass Transf.* **2022**, *183*, 122205. [[CrossRef](#)]
10. Altwieb, M.; Mishra, R.; Aliyu, A.M.; Kubiak, K.J. Heat Transfer Enhancement by Perforated and Louvred Fin Heat Exchangers. *Energies* **2022**, *15*, 400. [[CrossRef](#)]
11. Luo, W.; Yang, Z.; Jiao, K.; Zhang, Y.; Du, Q. Novel structural designs of fin-tube heat exchanger for PEMFC systems based on wavy-louvered fin and vortex generator by a 3D model in OpenFOAM. *Int. J. Hydrog. Energy* **2022**, *47*, 1820–1832. [[CrossRef](#)]
12. Song, K.W.; Hu, D.L.; Zhang, Q.; Zhang, K.; Wu, X.; Wang, L.B. Thermal-hydraulic characteristic of a novel wavy fin-and-circle tube heat exchanger with concave curved vortex generators. *Int. J. Heat Mass Transf.* **2022**, *194*, 123023. [[CrossRef](#)]
13. Jalil, E.; Goudarzi, K. Heat transfer enhancement of finned-tube heat exchanger using nozzle- and diffuser-shaped fins instead of straight fins. *Heat Transf.* **2022**, *51*, 1336–1357. [[CrossRef](#)]
14. Li, X.; Wang, H.; Luo, B. The thermophysical properties and enhanced heat transfer performance of SiC-MWCNTs hybrid nanofluids for car radiator system. *Colloids Surf. A Physicochem. Eng. Asp.* **2021**, *612*, 125968. [[CrossRef](#)]
15. Abbas, F.; Ali, H.M.; Shaban, M.; Janjua, M.M.; Shah, T.R.; Doranehgar, M.H.; Ahmadelouydarab, M.; Farukh, F. Towards convective heat transfer optimization in aluminum tube automotive radiators: Potential assessment of novel Fe<sub>2</sub>O<sub>3</sub>-TiO<sub>2</sub>/water hybrid nanofluid. *J. Taiwan Inst. Chem. Eng.* **2021**, *124*, 424436. [[CrossRef](#)]
16. Xian, H.W.; Sidik, N.A.C.; Saidur, R. Hybrid nanocoolant for enhanced heat transfer performance in vehicle cooling system. *Int. Commun. Heat Mass Transf.* **2022**, *133*, 105922. [[CrossRef](#)]
17. Li, D.; Yang, X.; Wang, S.; Duan, D.; Wan, Z.; Xia, G.; Liu, W. Experimental research on vibration-enhanced heat transfer of fin-tube vehicle radiator. *Appl. Therm. Eng.* **2020**, *180*, 115836. [[CrossRef](#)]
18. Legay, M.; Gondrexon, N.; Person, S.L.; Boldo, P.; Bontemps, A. Enhancement of Heat Transfer by Ultrasound: Review and Recent Advances. *Int. J. Chem. Eng.* **2011**, *2011*, 670108. [[CrossRef](#)]
19. Dehbani, M.; Rahimi, M.; Rahimi, Z. A review on convective heat transfer enhancement using ultrasound. *Appl. Therm. Eng.* **2022**, *208*, 118273. [[CrossRef](#)]
20. Amiri Delouei, A.; Sajjadi, H.; Ahmadi, G.A. Ultrasonic Vibration Technology to Improve the Thermal Performance of CPU Water-Cooling Systems: Experimental Investigation. *Water* **2022**, *14*, 4000. [[CrossRef](#)]
21. Amiri Delouei, A.; Atashafrooz, M.; Sajjadi, H.; Karimnejad, S. The thermal effects of multi-walled carbon nanotube concentration on an ultrasonic vibrating finned tube heat exchanger. *Int. Commun. Heat Mass Transf.* **2022**, *135*, 106098. [[CrossRef](#)]
22. Delouei, A.A.; Sajjadi, H.; Mohebbi, R.; Izadi, M. Experimental study on inlet turbulent flow under ultrasonic vibration: Pressure drop and heat transfer enhancement. *Ultrason. Sonochemistry* **2019**, *51*, 151–159. [[CrossRef](#)] [[PubMed](#)]
23. Delouei, A.A.; Sajjadi, H.; Izadi, M.; Mohebbi, R. The simultaneous effects of nanoparticles and ultrasonic vibration on inlet turbulent flow: An experimental study. *Appl. Therm. Eng.* **2019**, *146*, 268–277. [[CrossRef](#)]
24. Neethu, T.S.; Sabu, A.S.; Mathew, A.; Wakif, A.; Areekara, S. Multiple linear regression on bioconvective MHD hybrid nanofluid flow past an exponential stretching sheet with radiation and dissipation effects. *Int. Commun. Heat Mass Transf.* **2022**, *135*, 106115. [[CrossRef](#)]

25. Harfouf, E.I.; Wakif, A.; Mounir, S. Hayani Heat Transfer Analysis on Squeezing Unsteady MHD Nanofluid Flow Between Two Parallel Plates Considering Thermal Radiation, Magnetic and Viscous Dissipations Effects a Solution by Using Homotopy Perturbation Method. *Sens. Lett.* **2020**, *18*, 113–121. [[CrossRef](#)]
26. Nazari, M.; Ashouri, M.; Kayhani, M.H.; Tamayol, A. Experimental study of convective heat transfer of a nanofluid through a pipe filled with metal foam. *Int. J. Therm. Sci.* **2015**, *88*, 33–39. [[CrossRef](#)]
27. Moffat, R.J. Describing the uncertainties in experimental results. *Exp. Therm. Fluid Sci.* **1988**, *1*, 3–17. [[CrossRef](#)]
28. Bergman, T.L.; Lavine, A.S.; Incropera, F.P.; Dewitt, D.P. *Fundamentals of Heat and Mass Transfer*; John Wiley & Sons: Hoboken, NJ, USA, 2011.
29. Zhou, D.; Liu, D.; Hu, X.; Ma, C. Effect of acoustic cavitation on boiling heat transfer. *Exp. Therm. Fluid Sci.* **2002**, *26*, 931–938. [[CrossRef](#)]
30. Dorabialska, A.; Bankowski, K. *Poradnik Fizykochemiczny*; WNT: Warszawa, Warsaw, 1974.

**Disclaimer/Publisher’s Note:** The statements, opinions and data contained in all publications are solely those of the individual author(s) and contributor(s) and not of MDPI and/or the editor(s). MDPI and/or the editor(s) disclaim responsibility for any injury to people or property resulting from any ideas, methods, instructions or products referred to in the content.